Wang, L.; Pyczak, F.; Zhang, J.; Lou, L.H.; Singer, R.F.:

Effect of eutectics on plastic deformation and subsequent recrystallization in the single crystal nickel base superalloy CMSX-4

In: Materials Science and Engineering A (2011) Elsevier

DOI: 10.1016/j.msea.2011.11.015

Effect of eutectics on plastic deformation and subsequent recrystallization in the single crystal nickel base superalloy CMSX-4

L. Wang[a,b,*], F. Pyczak[c], J. Zhang[a], L.H. Lou[a], R.F. Singer[b]

[a] *Institute of Metal Research, Chinese Academy of Sciences, No. 72, Wenhua Road, Shenyang 110016, China*

[b] *Erlangen-Nuremberg University, Martensstr. 5, Erlangen 91058, Germany*

[c] *Helmholtz-Zentrum Geesthacht, Max-Planck-Strasse 1, Geesthacht 21502, Germany*

Abstract

The Electron Backscattered Diffraction (EBSD) technique and transmission electron microscopy (TEM) were used to characterize the microstructure of a locally deformed single crystal (SX) nickel-base superalloy – CMSX-4. The effect of eutectics on the deformation and recrystallization (RX) behavior was investigated. It was found that the texture component map is a reliable method for the determination of the severity of deformation in locally deformed SX superalloys. Severe deformation was mainly created in interdendritic regions, especially around eutectics. The dislocation distribution and configuration was consistent with the nucleation and the growth behavior of recrystallizing grains.

Keywords:

Single crystal (SX) superalloy; Recrystallization (RX); Eutectics; Indentation; Dislocation

Introduction

To avoid recrystallization (RX) is one of the major difficulties in the post casting process of directionally solidified (DS) or single crystal (SX) superalloys. In recent years, due to its detrimental effect on mechanical properties [1-6], much attention had been paid on RX

* Corresponding author at: Superalloys Division, Institute of Metal Research, Chinese Academy of Sciences, No. 72, Wenhua Road, Shenyang 110016, China

Tel.: +86-24-23971276, Fax: +86-24-23971712, E-mail: wangli@imr.ac.cn (L. Wang)

in DS and especially SX superalloys [4, 7-10].

As RX is very sensitive to second phase particles or microstructural inhomogeneities [11], and eutectics are one of the most inhomogeneous microstructure components in SX superalloys, the role of eutectics during RX in locally indented and heat treated SX superalloy was studied in one of our previous papers [12]. It was found that eutectics play an important role during nucleation and growth of RX grains. They act as second phase particles to stimulate RX nucleation by a particle stimulated nucleation (PSN) mechanism in the interdendritic regions. In the areas just below the indent, RX nucleation is found to occur within and around eutectics simultaneously. During RX grain growth eutectics exhibited different interactions with moving grain boundaries: Eutectics pinned the advancing RX grain boundary in areas far below the indent. In areas close to the indent, RX grain boundaries migrated right through eutectics forming a large γ′ phase in their wake [12].

Though these phenomena were observed, the mechanisms still remain unclear. According to Chaudhri and Wang et al.'s study [13, 14], significant plastic strain could be generated below a spherical indent and other studies show that the intermetallic Ni_3Al phase can be deformed and a high density of dislocations can be generated in its interior at room temperature if the stress and strain is sufficiently high [15-17]. As locally indented SX superalloys are concerned, in theory the plastic deformation is well known as Zambaldi et. al. [18] simulated the residual strain distribution around a spherical indentation on the sample surface and the resulting recrystallized region in the material showed a good agreement between simulation and experiment. There were also many researchers who reported the dislocation configuration in deformed superalloys [19-22], but most of them focused on the deformation in the matrix phase not in the areas around or within large γ/γ′ eutectics.

As had been reported in our previous work [12] a strong concentration of plastic deformation was found by local misorientation measurements using electron backscattered diffraction (EBSD) in these eutectic regions. Accordingly it is understandable that PSN can be promoted by the presence of eutectics. Nevertheless more detailed investigations are necessary to understand under which conditions eutectics pin migrating RX grain

boundaries while eutectics themselves undergo RX in other cases. For this and to reaffirm that the concentration of plastic deformation around eutectics make them nucleation sites for RX, the distribution and severity of deformation below an indent is characterized in more detail here. Therefore, as-deformed and as-cast SX samples were investigated by EBSD and transmission electron microscopy (TEM) in the present paper. Details of the deformation structure, such as dislocation configuration below the indent were studied and correlated to the RX behavior.

Experimental procedure

The alloy investigated here is the commercially available SX alloy CMSX-4. Samples were cut from the CMSX-4 slab into cubes of $10\times10\times10$ mm^3. Electron discharge machining (EDM) was employed for cutting in order to avoid additional surface deformation.

These samples were indented on a surface parallel to the crystallographic (100) plane by a spherical indenter of 5 mm in diameter with a load of 14.7 kN for 10 s (for specimen geometry see Fig. 1). One group of indented samples was subsequently heat treated at 1290 ^{o}C for 8 h, for the investigation of the recrystallization (RX) behavior. The other group of deformed samples was cut right across the diameter of the indentation and vertical to the solidification direction (plane with dashed outline marked in Fig. 1). These samples were mechanically polished and examined by electron backscattered diffraction (EBSD) (a Zeiss Crossbeam 1540 ESB with Nordlys II detector and software Channel 5 was used for this analysis), or polished and etched for microstructure observation.

In order to observe the dislocation morphology at different distances below the indent, a small column with a diameter of 4 mm was cut from the specimen as shown in Fig. 1. This column was then cut in slices along the (100) plane every 600 μm beginning from the bottom of the indentation. These samples were grinded and then thinned by twin jet polishing with an etchant of 10% perchloric acid in ethanol to electron transparency. The dislocation distribution and configuration in different areas were studied by transmission

electron microscopy (TEM) (Philips TECNAI 20) and correlated with the RX nucleation and grain growth behavior.

Results

The investigation of samples annealed at 1290 ^{o}C by optical microscopy (Fig. 2) shows large RX areas under the indentation site. A texture component map of the area below the indent in an as-deformed specimen is shown in Fig. 3a. The shape of the deformed area in the texture component map is similar to the shape of the recrystallized area of the heat treated samples in Fig. 2. The maximum depth of RX is consistent with the area where a misorientation component could still be detected.

The misorientation profile along line AB marked in Fig. 3a is shown in Fig. 3b. The accumulated misorientation increases sharply from directly below the indent and reaches the maximum value around 500 μm deeper.

A higher magnification of an area located about 900 μm below the indent in an as-deformed sample is shown in Fig. 4. The area marked ABCD in the optical micrograph in Fig. 4a was analyzed by EBSD. The corresponding local misorientation map is shown in Fig. 4b. The deformation is especially pronounced in the interdendritic regions where eutectics are located (Fig. 4b). From the misorientation profile along the line marked EF in Fig. 4b, which is plotted in Fig. 4c, it can be seen that the maximum accumulative misorientation is about 12 degree. This is nearly as high as the maximum value recorded in Fig. 3b.

TEM images from the same area are shown in Fig. 5. A high density of dislocations was observed within γ channels (Fig. 5a), large γ′ phase in γ/γ′ eutectics (Fig. 5b) and at the interfaces between eutectics and the matrix (Fig. 5c). Stacking faults were recorded occasionally within γ′ phase as marked by arrows in Fig. 5a. These stacking faults are comparatively rare and are not extended over more than one γ′ precipitate.

In the area about 1500 μm below the indent of the as-deformed samples, the local misorientation was also pronounced around the interdendritic γ/γ′ eutectics (see Fig. 6b, local misorientation map of region ABCD in Fig. 6a). Nevertheless, according to the

accumulative misorientation profile recorded along the line EF in Fig. 6b, which is shown in Fig. 6c, the maximum accumulative misorientation is rather small with about 4 degree compared to regions located nearer to the indent.

A detailed investigation of the same area by TEM shows that the deformation is mostly confined within γ matrix channels (Fig. 7a). Dislocation pairs were observed in the γ′ phase of the γ/γ′ eutectics, and the dislocation density is high along the interface between eutectic and matrix and along the γ channels within γ/γ′ eutectics (Fig. 7b). But qualitatively the dislocation density appears to be much lower than at the position closer to the indent (compare with Fig. 5 a, b and c).

In the as-cast samples, no misorientation was detected as shown in Fig. 8. From the misorientation profiles along line AB in Fig. 8a and b, one can tell that the maximum accumulative misorientation is only about 0.55 degree (Fig. 8c).

This is also supported by the fact that only occasionally dislocations could be observed in the γ matrix channels in this region (Fig. 9).

Discussion

The good agreement between the texture component map of the deformed sample (Fig. 3a) and the RX areas in the heat treated sample (Fig. 2) indicates that EBSD is a reliable method to determine the severity of the deformation in the as-deformed SX superalloys. The RX nucleation and grain growth behavior is closely related to the location and severity of plastic deformation detected by EBSD measurements.

Now we will relate the observed levels of plastic deformation and the present dislocation structures at different distances below the indent in more detail to the observed RX behavior in these regions. In the area about 900 μm below the indent, due to the significant increase in dislocation density at eutectic/matrix interfaces and within eutectics a high amount of stored energy [15] is present to act as driving force for RX nucleation. Similar conditions are also present in the area around 1500 μm below the indent where, according to the local misorientation map, plastic strain is still concentrated around eutectics. This is consistent with the result of the TEM observation. A high density of

dislocations was observed along the interface between γ/γ′ eutectics and the adjacent matrix (Fig. 7b), which leads to the nucleation of RX grains around the eutectics by a PSN mechanism during the following annealing [12].

Though PSN is a feature found for all eutectics present in the deformed zone, the interaction of γ/γ′ eutectics with moving RX grain boundaries is a different matter. Closely below the indent, RX grain boundaries migrate through the γ/γ′ eutectic, forming a γ′ particle in the γ/γ′ eutectic region during this process [12]. Farther away from the indent, eutectic γ′ phase does not undergo a RX process itself but in this case pins a RX grain boundary migrating through the adjacent matrix phase [12]. This different behavior can be understood by the different levels of strain energy stored within and around the γ/γ′ eutectic.

As known from the literature, a high level of deformation is generated just below a spherical indent [13, 14] and intermetallic Ni_3Al phases are deformable at room temperature if the stresses and strains are high enough [15-17]. It is therefore reasonable to assume that γ′ precipitates are deformed at room temperature as observed here in areas directly below the indent with a high level of deformation. Accordingly a corresponding high density of dislocations was also observed in the eutectic γ′ phase as well as in eutectic γ phase at a short distance below the indent. Due to the high density of dislocations (high stored energy) within γ/γ′ eutectic there exists a significant driving force for the RX of the eutectics themselves under these conditions. And this will also favor the migration of grain boundaries into γ/γ′ eutectics [12].

The situation is different in regions farther away from the indent. Here the deformation energy stored within γ/γ′ eutectic is too low to act as sufficient driving force for RX to occur in the γ/γ′ eutectic itself. Also the eutectic has most probably a favorable crystallographic orientation with respect to the surrounding grain [23, 24]. This favorable crystallographic relation does not exist with respect to a new RX grain and the deformation energy stored in the γ/γ′ eutectic is not sufficiently high to undergo RX itself and adapt to the new situation in this way. That is why a γ/γ′ eutectic in this region pins the migrating RX grain boundary to avoid being enclosed by the new RX grain.

Summary

The effect of eutectics on the deformation and recrystallization (RX) behavior in the single crystal (SX) superalloy CMSX-4 was studied in the present paper. The results can be summarized as follows:

1. The deformation of SX alloys under the indentation is heterogeneous. Macroscopically, the most severe deformation was found in an area about 500~1000 μm below the indent. Locally, the areas near γ/γ′ eutectics in interdendritic regions exhibit the most severe deformation.
2. The RX nucleation and grain growth behavior are closely related to the dislocation distribution and configuration in the different areas. The high dislocation density in eutectic γ′ and at eutectic/matrix interfaces promotes the nucleation of RX grains.
3. Eutectics interact differently with migrating RX grain boundaries. If the dislocation density within γ/γ′ eutectics is high enough the eutectics themselves undergoes RX when a RX grain boundary moves by. If the dislocation density in the γ/γ′ eutectics is low the RX grain boundary is pinned at the eutectic.

Acknowledgement

This work was partly supported by the National Basic Research Program of China (Grant NO. 2010CB631201) and National Natural Science Foundation of China (Grant NO. 50931004). The authors are grateful for these supports.

References

[1] B. Ralph, C. Barlow, B. Cooke, A. Porter, Proc. 1st Risø Int. Symp. in Recrystallization, 1980, 229-241.

[2] T. Khan, P. Caron, Y.G. Nakagawa, J. Metal. 1986, 16-19.

[3] C.T. Sims, N.S. Stoloff, W.C. Hagel, Superalloy II, John Wiley & Sons, New York, 1987.

[4] U. Paul, P.R. Sahm, D. Goldschmidt, Mater. Sci. Eng. A173 (1993) 49-54.

[5] C.Y. Jo, H.M. Kim, Mater. Sci. Technol. 19 (2003) 1671-1676.

[6] G. Xie, L. Wang, J. Zhang, L.H. Lou, Metall. Mater. Trans. A. 39 (2008), 206-210.

[7] S.D. Bond, J.W. Martin, J. Mater. Sci. 19 (1984) 3867-3872.

[8] R. Bűrgel, P.D. Portella, J. Preuhs, Superalloys 2000, 2000, 229-238.

[9] D.C. Cox, B. Roebuck, C.M.F. Rae, R.C. Reed, Mater. Sci. Technol. 19 (2003) 440-446.

[10] C.Y. Jo, H.Y. Cho, H.M. Kim, Mater. Sci. Technol. 19 (2003) 1665-1670.

[11] F.J. Humphreys, M. Hatherly, Recrystallization and related annealing phenomena, second ed., Elsevier, Kidlington, 2004.

[12] L. Wang, F. Pyczak, J. Zhang, R.F. Singer, Inter. J. Mater. Res. 100 (2009) 1046-1051.

[13] A. Wang, U.J. De Souza, H.J. Rack, Wear. 151 (1991) 157-173.

[14] M. Munawar Chaudhri, Phil. Mag. A. 74 (1996) 1213-1224.

[15] I. Baker, J.W. Martin, Metal Sci. 17 (1983) 459-467.

[16] L.M. Hsiung, N.S. Stoloff, Acta Metall. Mater. 42 (1994) 1457-1467.

[17] T. Kruml, V. Paidar, J.L. Martin, Intermetallics. 8 (2000) 729-736.

[18] C. Zambaldi, F. Roters, D. Raabe, U. Glatzel, Mater. Sci. Eng. A. 454-455 (2007) 433-440.

[19] M. Dollar, I.M. Bernstein, Superalloys 1988, 1988, 275-284.

[20] M. Feller-Kniepmeier, T. Link, I. Poschmann, G. Scheunemann-Frerker, C. Schulze, Acta Mater. 44 (1996) 2397-2407.

[21] Z.P. Luo, Z.T. Wu, D.J. Miller, Mater. Sci. Eng. A354 (2003), 358-368.

[22] S.G. Tian, X.F. Yu, J.H. Yang, N.R. Zhao, Y.B. Xu, Z.Q. Hu, Mater. Sci. Eng. A. 379 (2004) 141-147.

[23] N. Warnken, D. Ma, M. Mathes, I. Steinbach, Mater. Sci. Eng. A. 413-414 (2005) 267-271.

[24] A. Heckl, R. Rettig, S. Cenanovic, M. Goeken, R.F. Singer, J. Cryst. Growth. 312 (2010) 2137-2144.

Figure captions:

Fig. 1 Schematic of indented sample

Fig. 2 Optical micrograph showing recrystallized area below the indent after annealing at 1290 ^{o}C for 8 h of an indented sample

Fig. 3 EBSD results of the area below the indent in the as-deformed specimen. (a) Texture component map of the area below the indent (orientation difference relative to position marked by O), and (b) accumulative misorientation profile along line AB in (a)

Fig. 4 EBSD results of the area about 900 μm below the indent in an as-deformed specimen. (a) Optical micrograph showing the analyzed area, (b) local misorientation map of the region marked ABCD in (a), (c) accumulative misorientation profile along line EF in (b)

Fig. 5 TEM results show dislocations in (a) matrix in interdendritic regions, (b) γ′-phase within eutectics and (c) along the interface between matrix and eutectics at a position about 900 μm below the indent in an as-deformed specimen

Fig. 6 EBSD results of an area about 1500 μm from the indent in an as-deformed specimen (the square dots are marks made by microhardness tester). (a) Optical micrograph showing the analyzed area, (b) local misorientation map of area ABCD in (a), and (c) accumulative misorientation profile along line EF in (b)

Fig. 7 Dislocation distribution in an area about 1500 μm below the indent in an as-deformed specimen: (a) Dislocations in matrix channels between γ′ particles, (b) dislocation pairs cutting through γ′ particles in eutectic regions and high density of dislocations located at the interface between γ/γ′ eutectics and the surrounding matrix

Fig. 8 EBSD results of as-cast specimen: (a) Microstructure pictured by scanning electron microscopy (SEM), (b) local misorientation map of the same area and (c) accumulative misorientation profile along line AB in (a)

Fig. 9 Dislocations in the matrix of the as-cast sample

Fig.1 Schematic of indented sample

Click here to download high resolution image

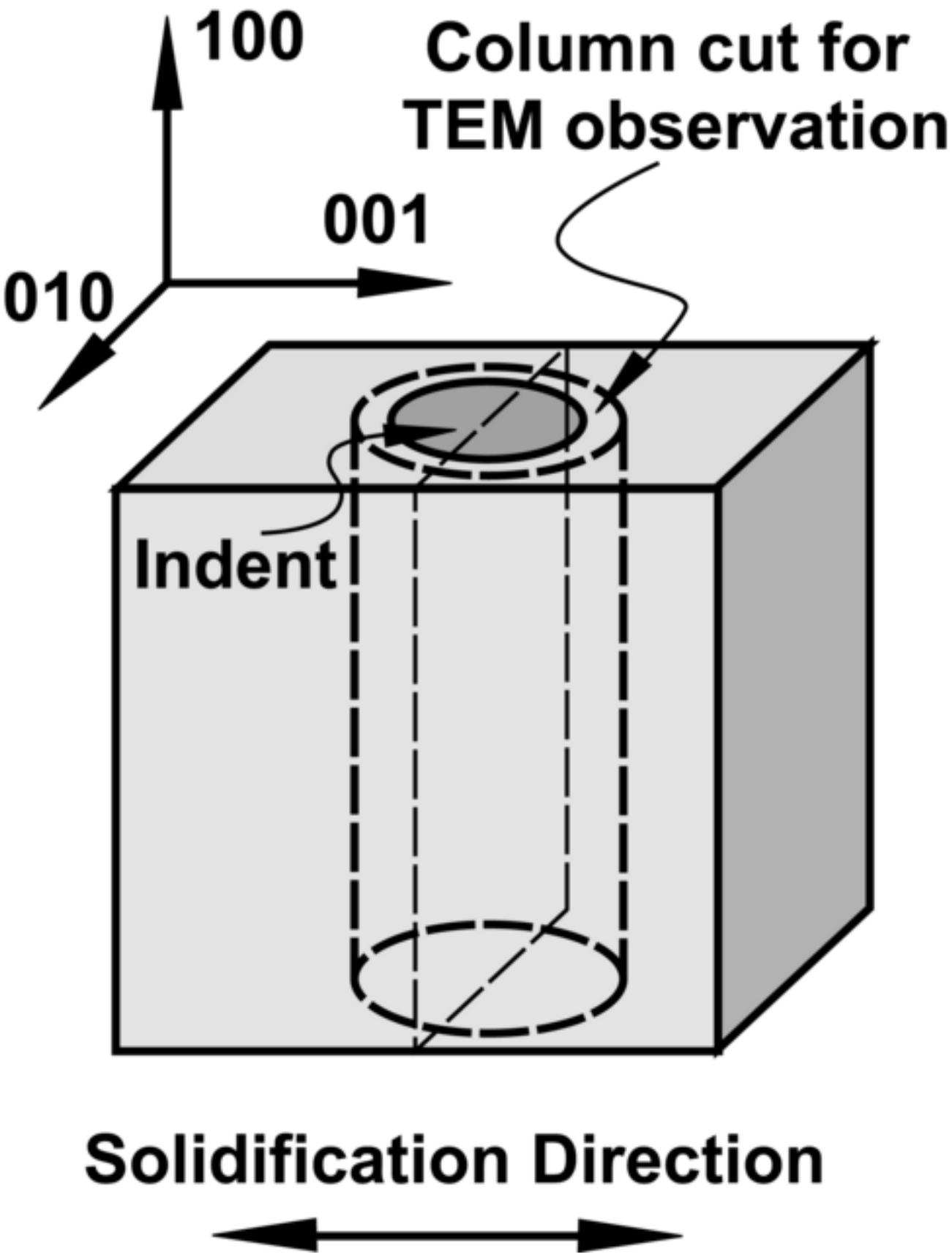

Fig.2 Recrystallized area below the indent

Click here to download high resolution image

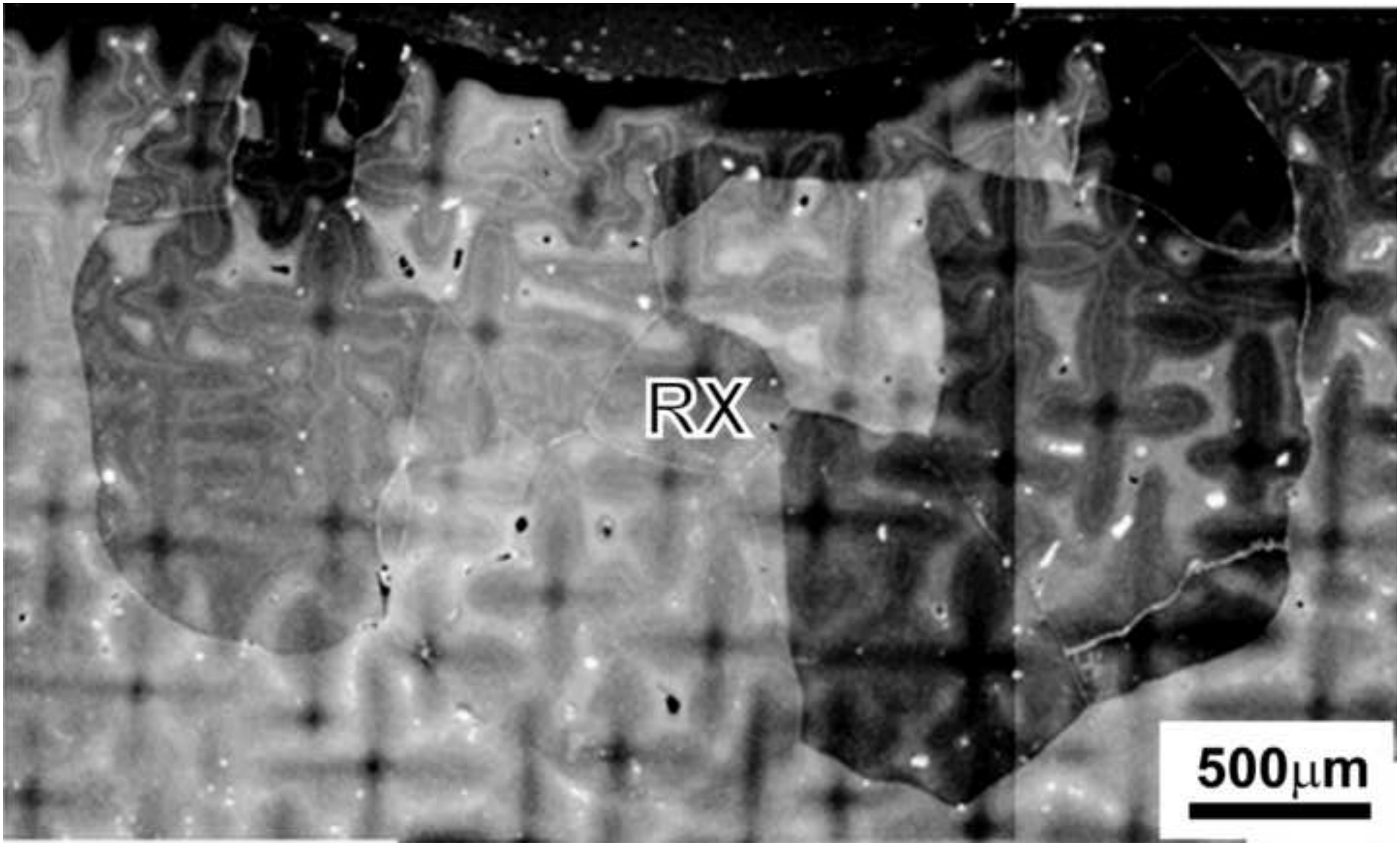

Fig.3a Texture component map below the indent
Click here to download high resolution image

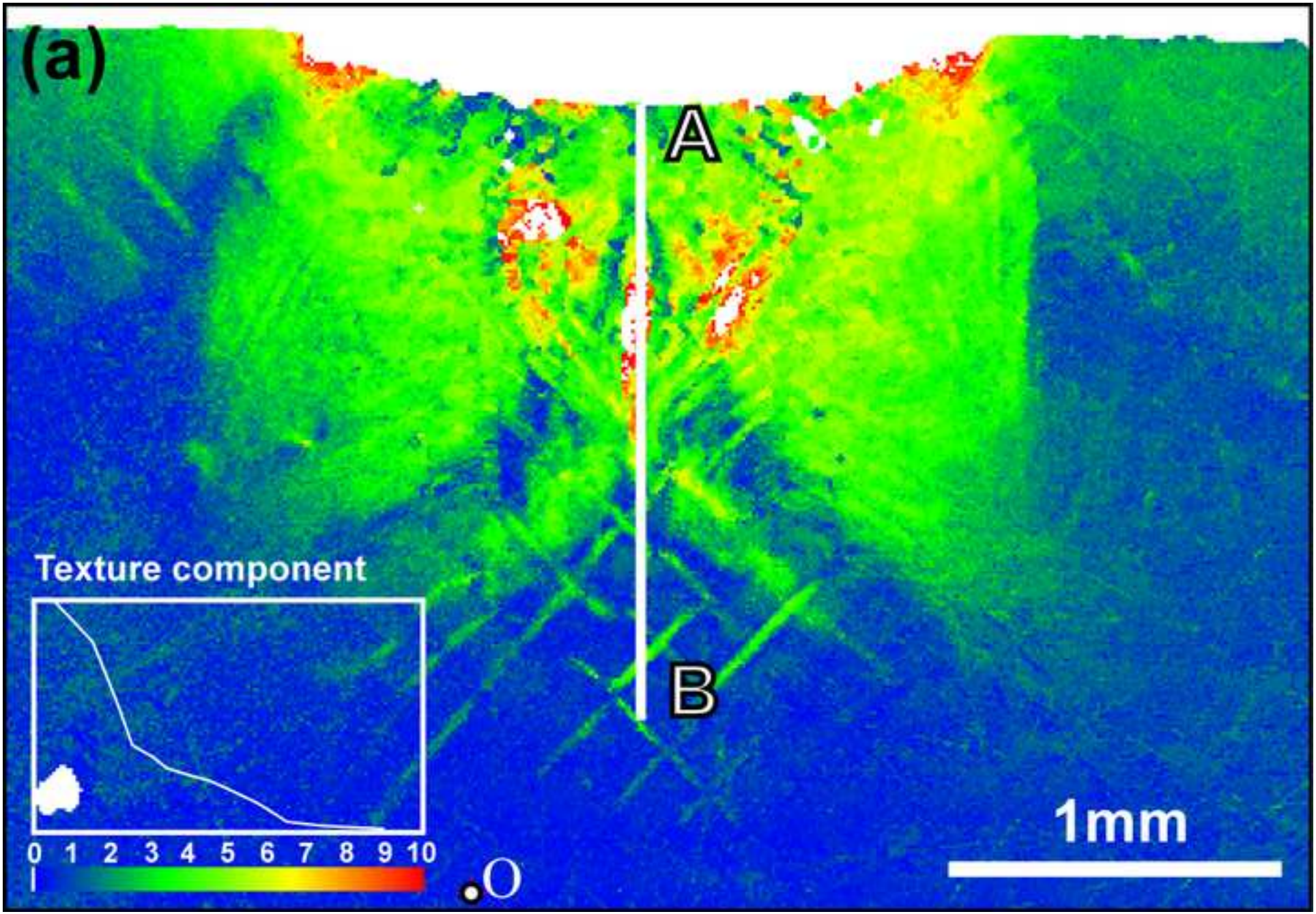

Fig.3b Accumulative misorientation profile along line AB in 3a

Click here to download high resolution image

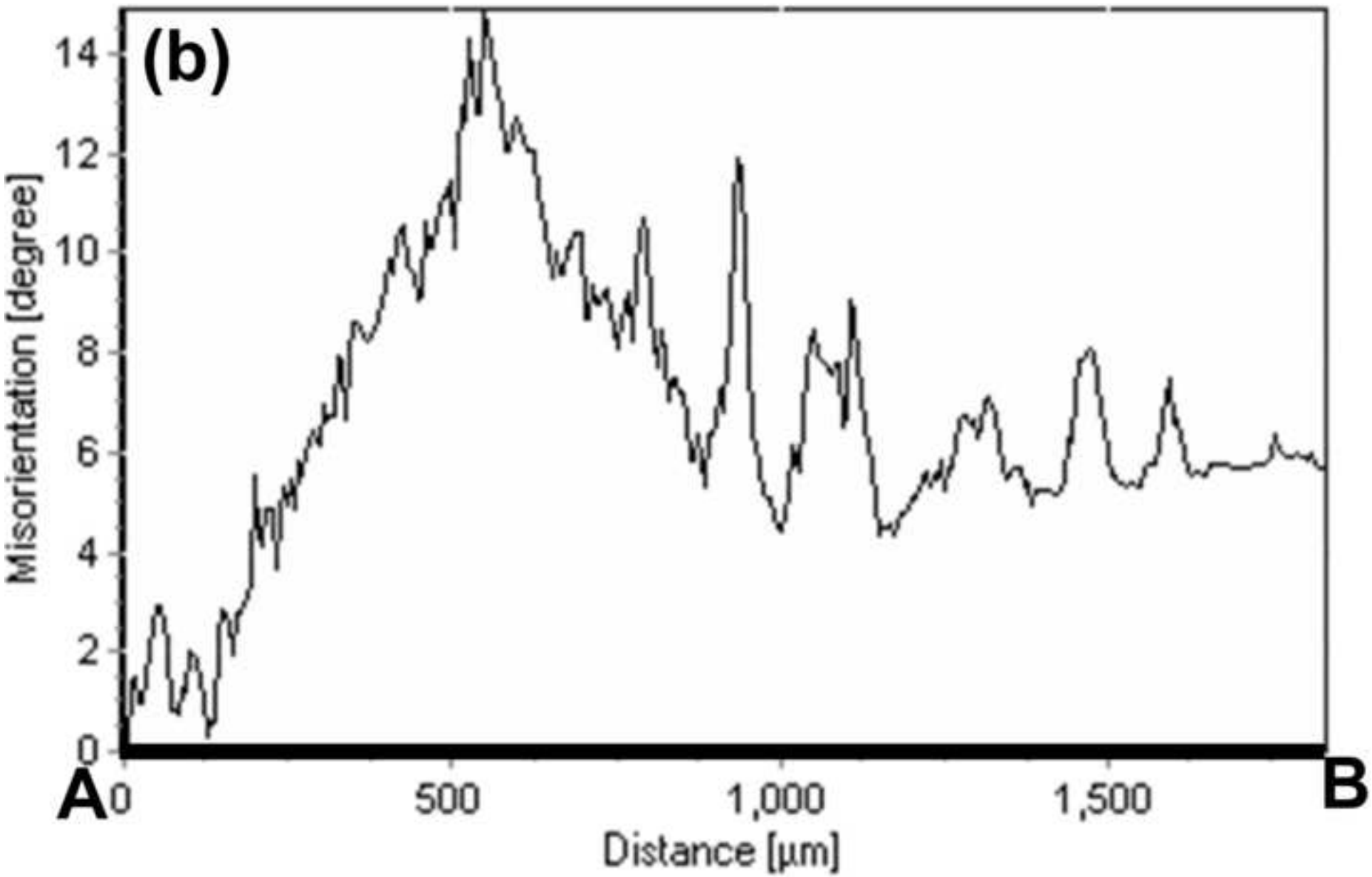

Fig.4a Area about 900 micron below the indent
Click here to download high resolution image

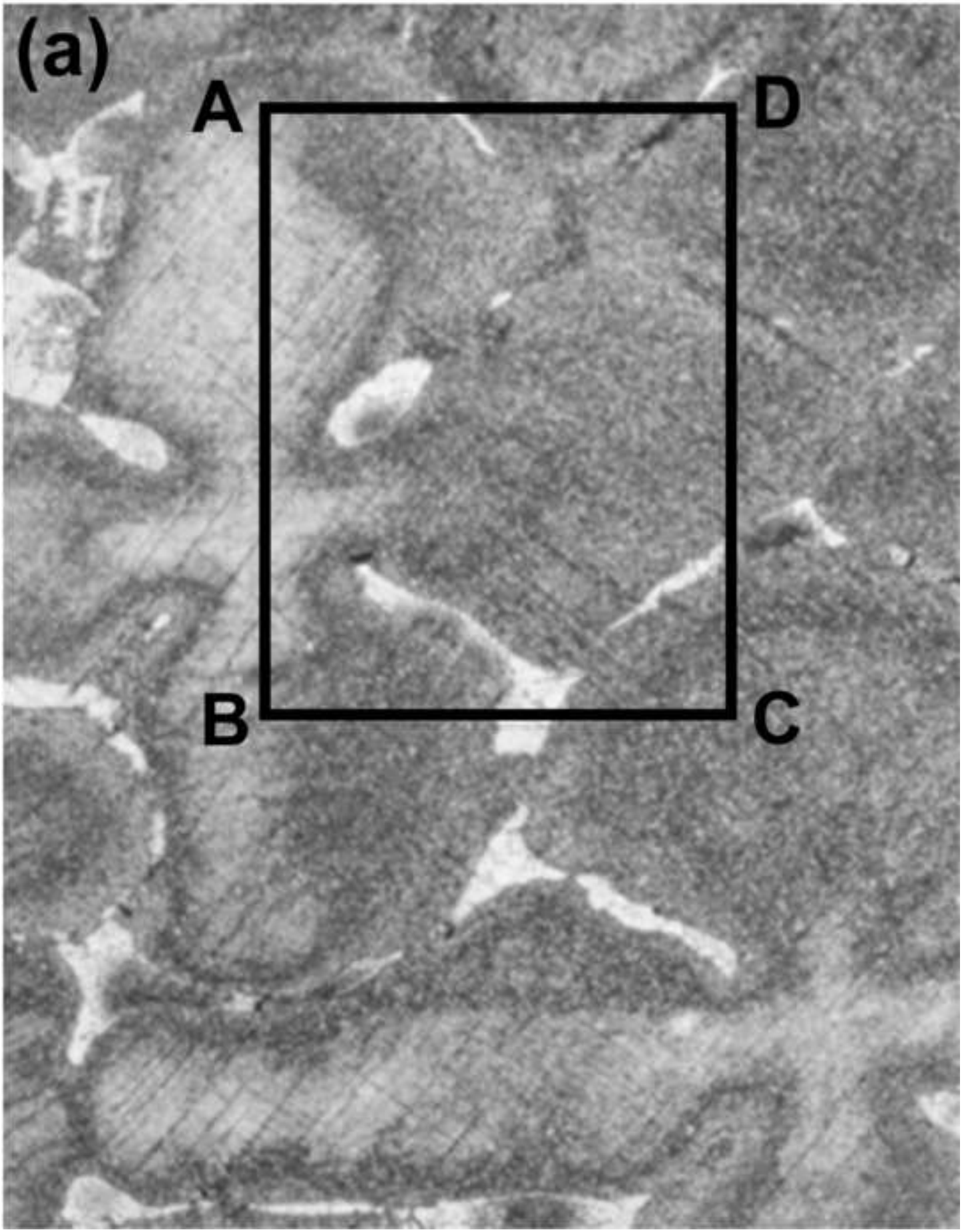

Fig.4b Local misorientation map of the region marked in Fig. 4a

Click here to download high resolution image

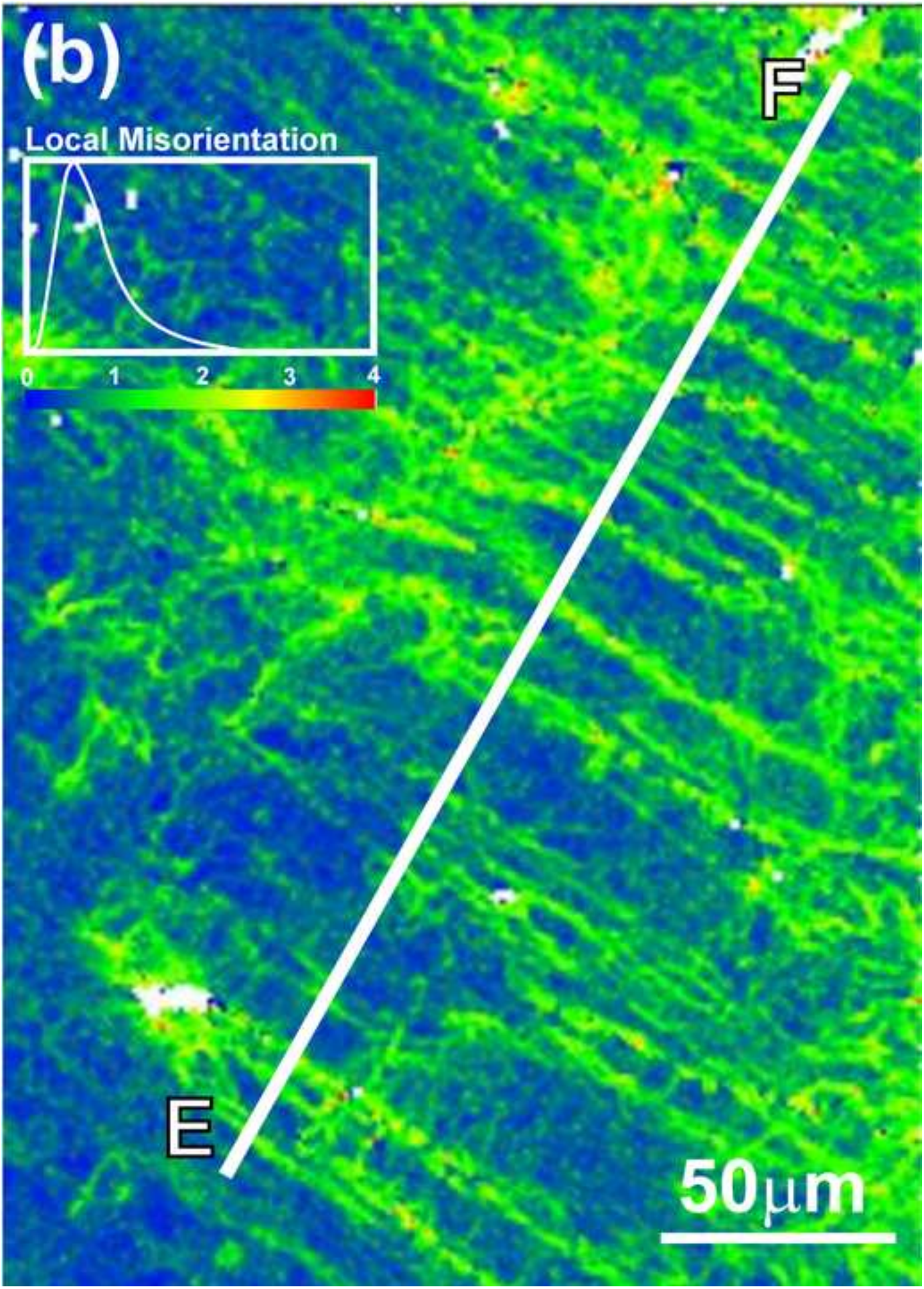

Fig.4c Accumulative misorientation profile along line EF in 4b

Click here to download high resolution image

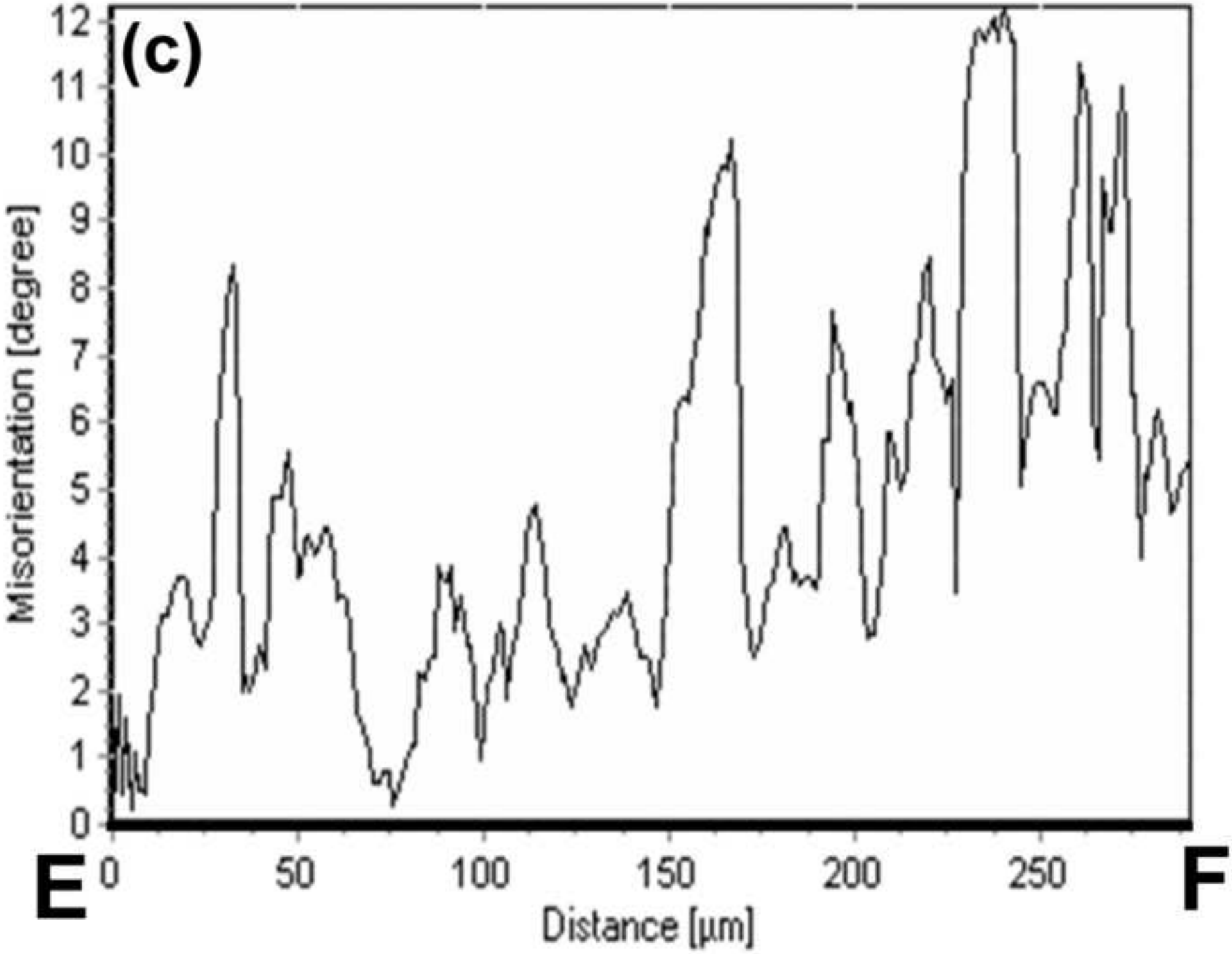

Fig.5a Dislocations in matrix about 900micron below the indent

Click here to download high resolution image

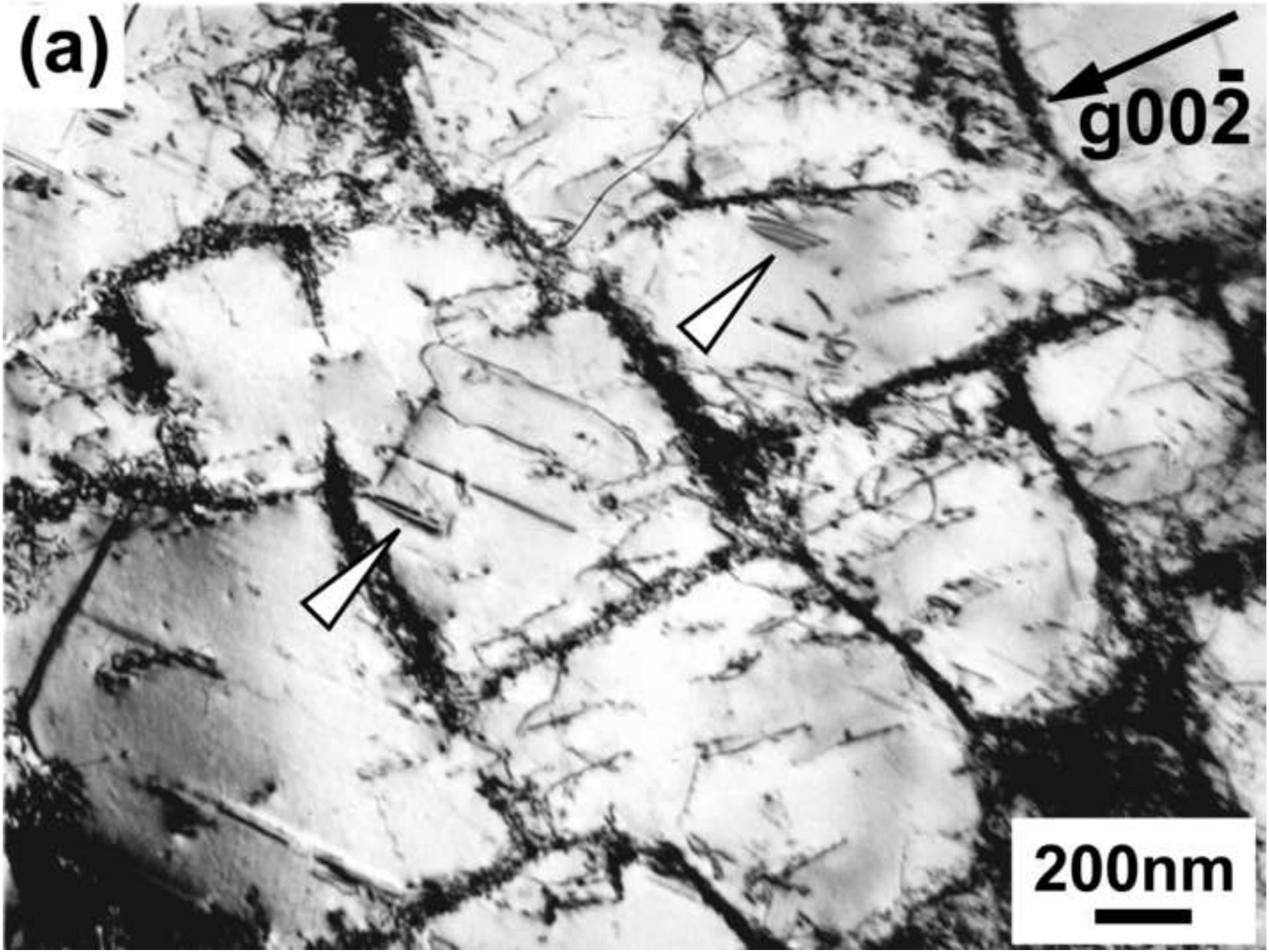

Fig.5b Dislocation in eutectics about 900micron below the indent

Click here to download high resolution image

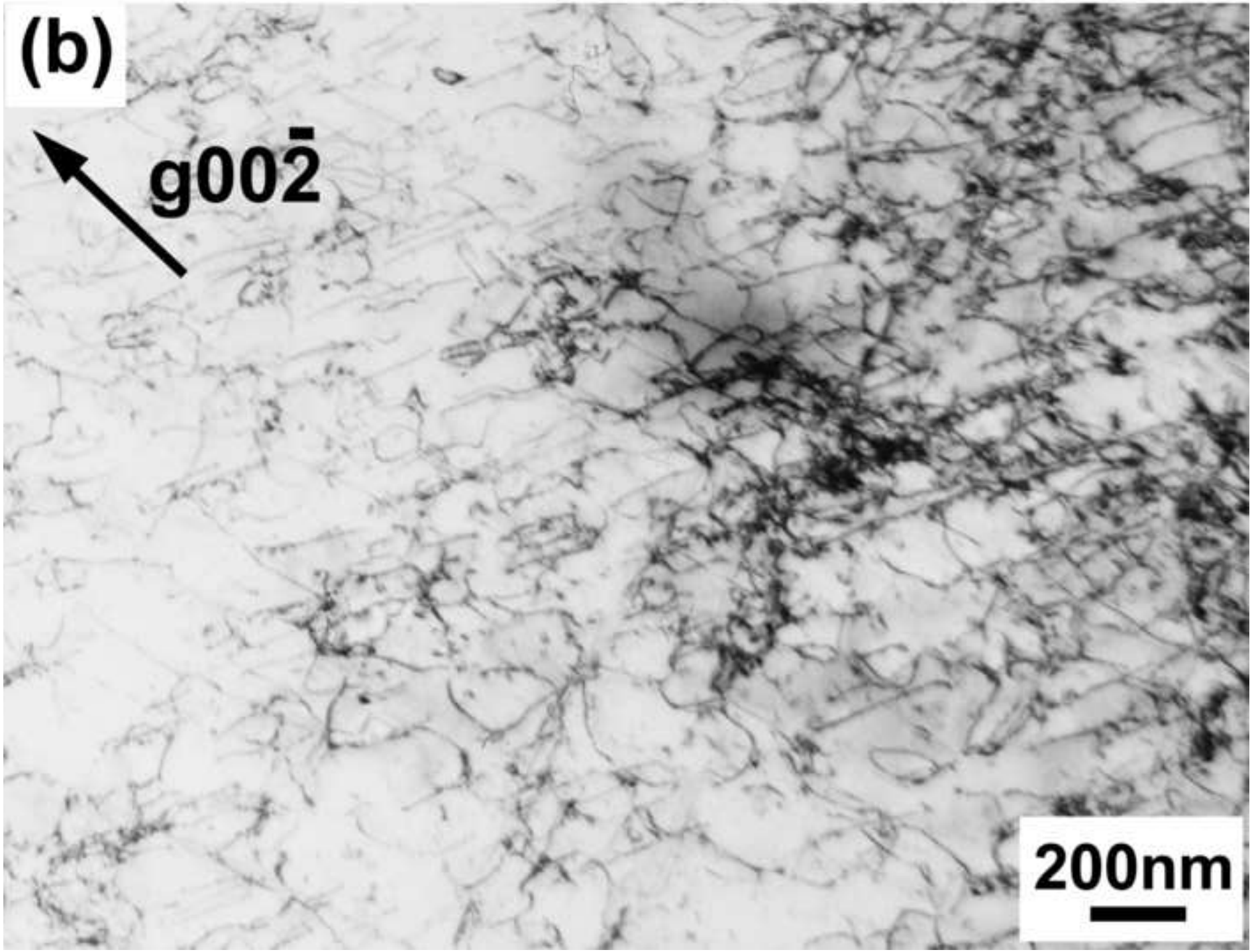

Fig.5cDislocation along the interface between matrix and eutecti

Click here to download high resolution image

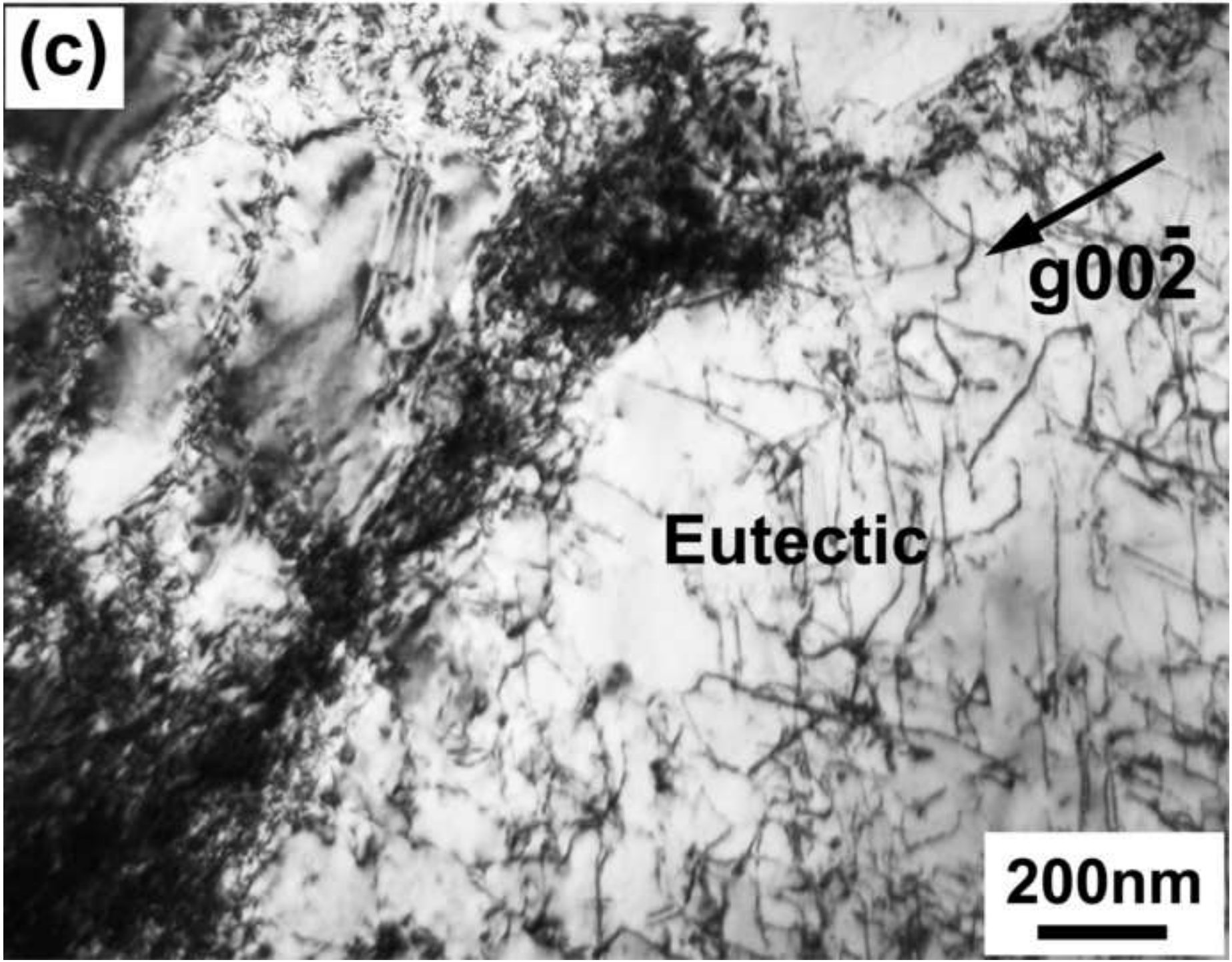

Fig.6a Area about 1500micron from the indent

Click here to download high resolution image

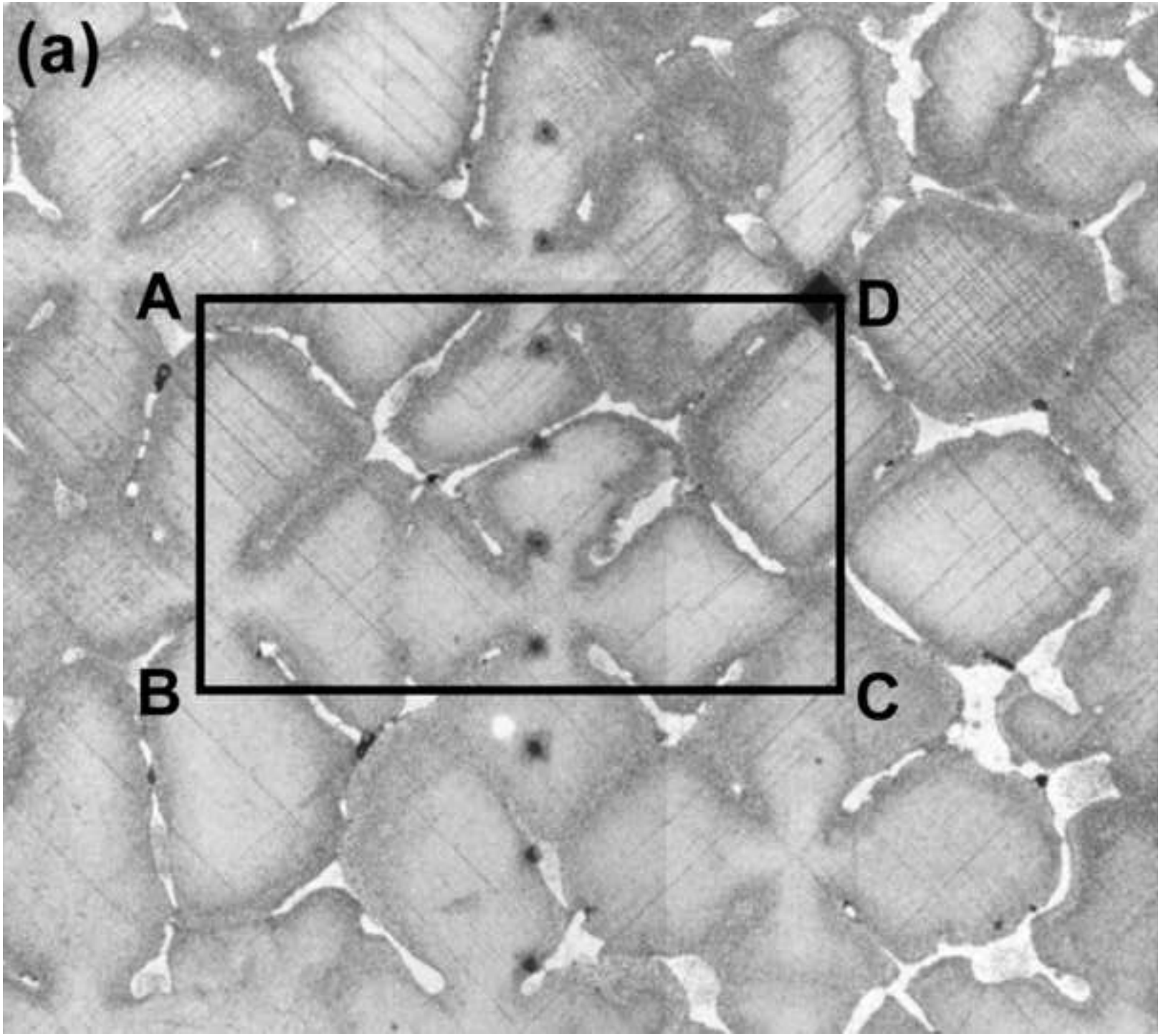

Fig.6b Local misorientation map of area ABCD in Fig. 6a
Click here to download high resolution image

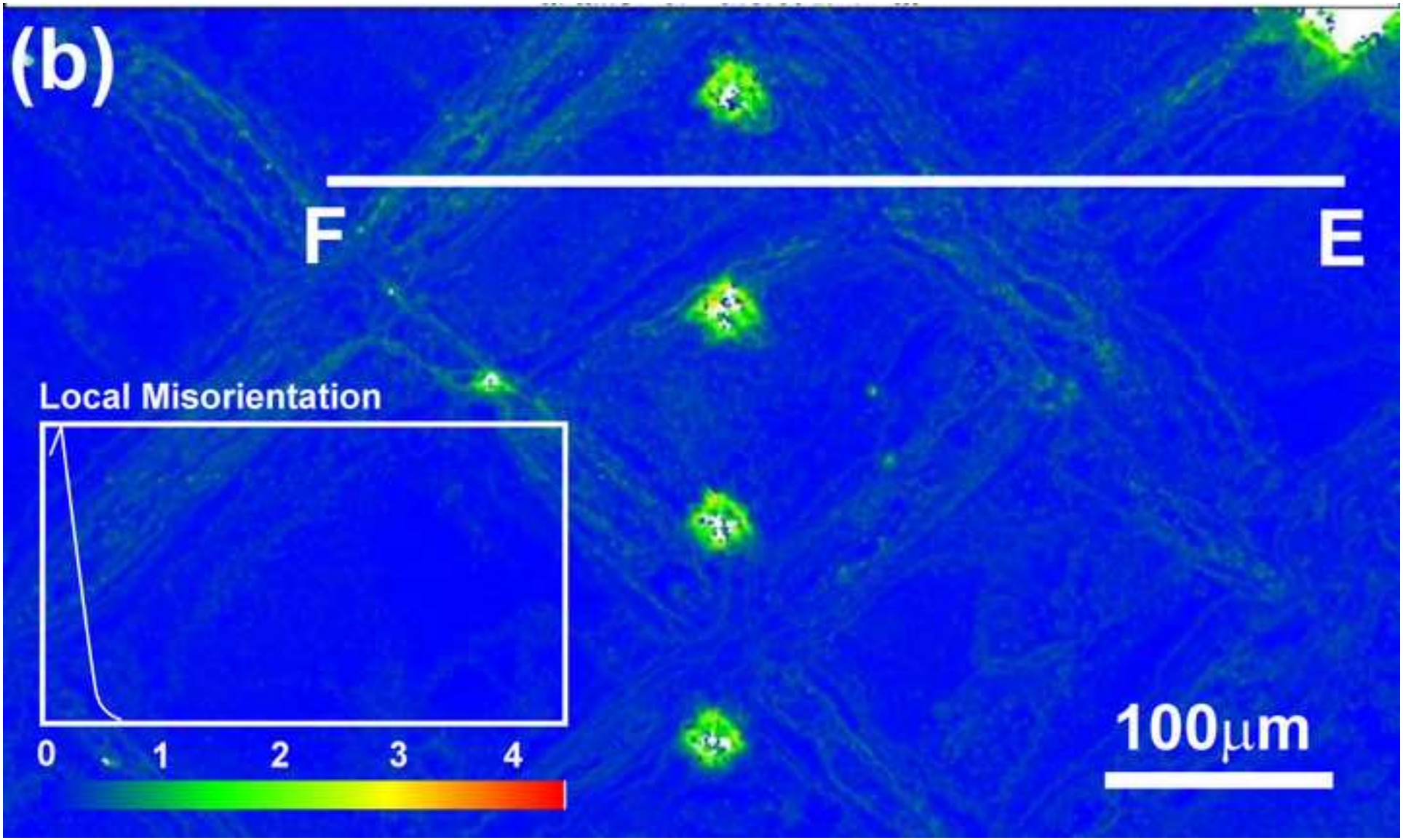

Fig.6c Accumulative misorientation profile along line EF in 6b

Click here to download high resolution image

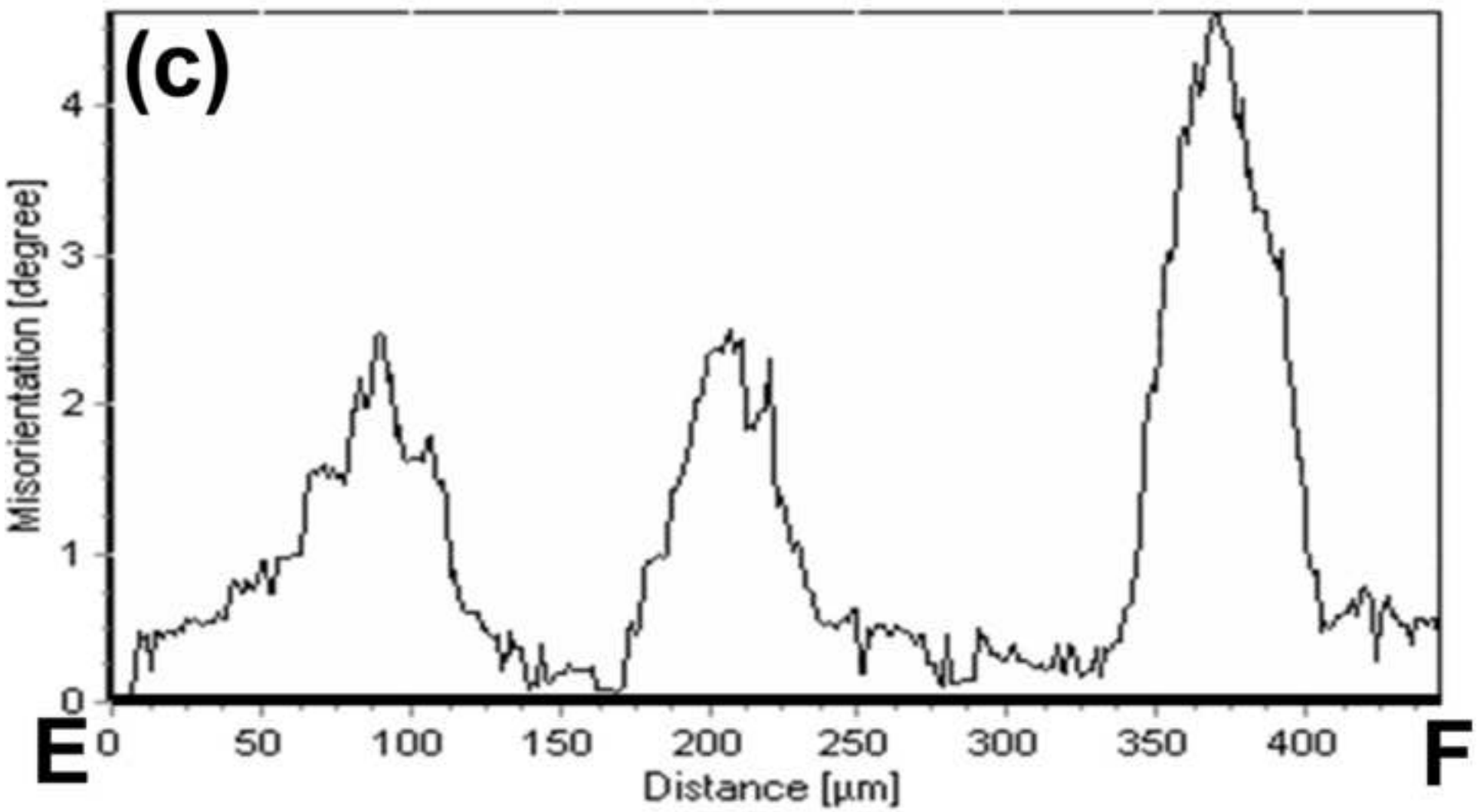

Fig.7a Dislocations in matrix about 1500micron below indent

Click here to download high resolution image

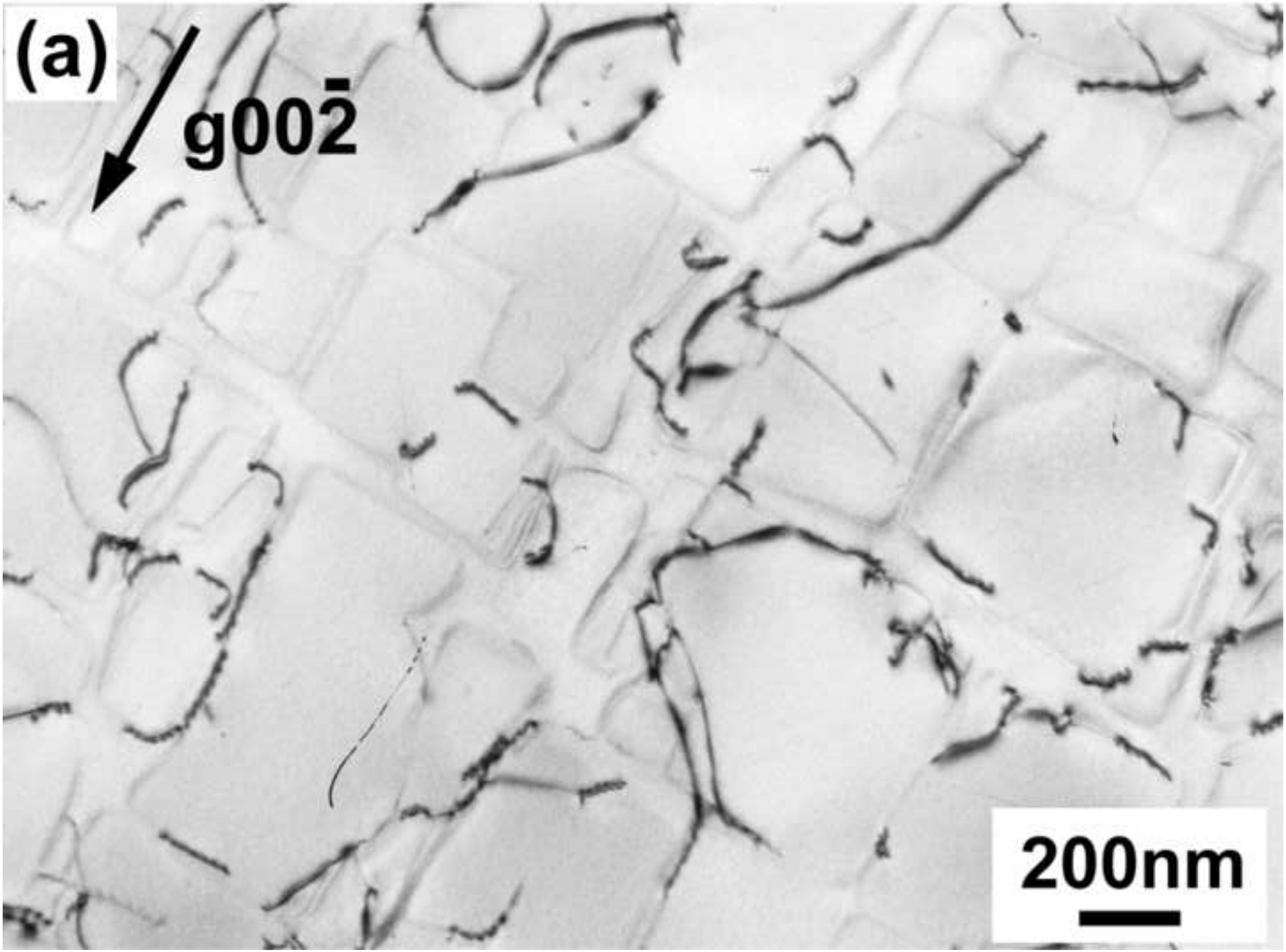

Fig.7b Dislocation around eutectics

Click here to download high resolution image

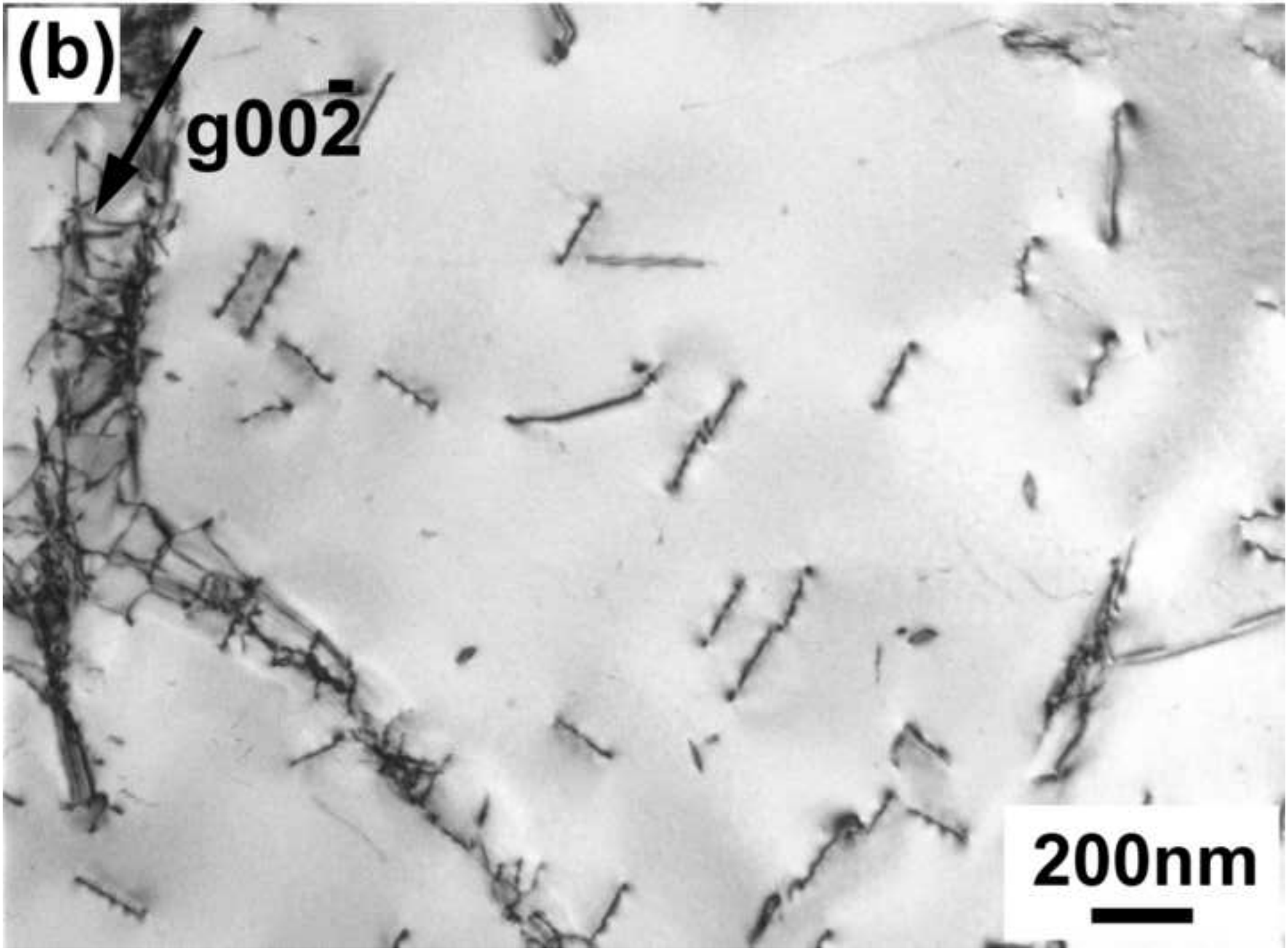

Fig.8a SEM image of as-cast specimen

Click here to download high resolution image

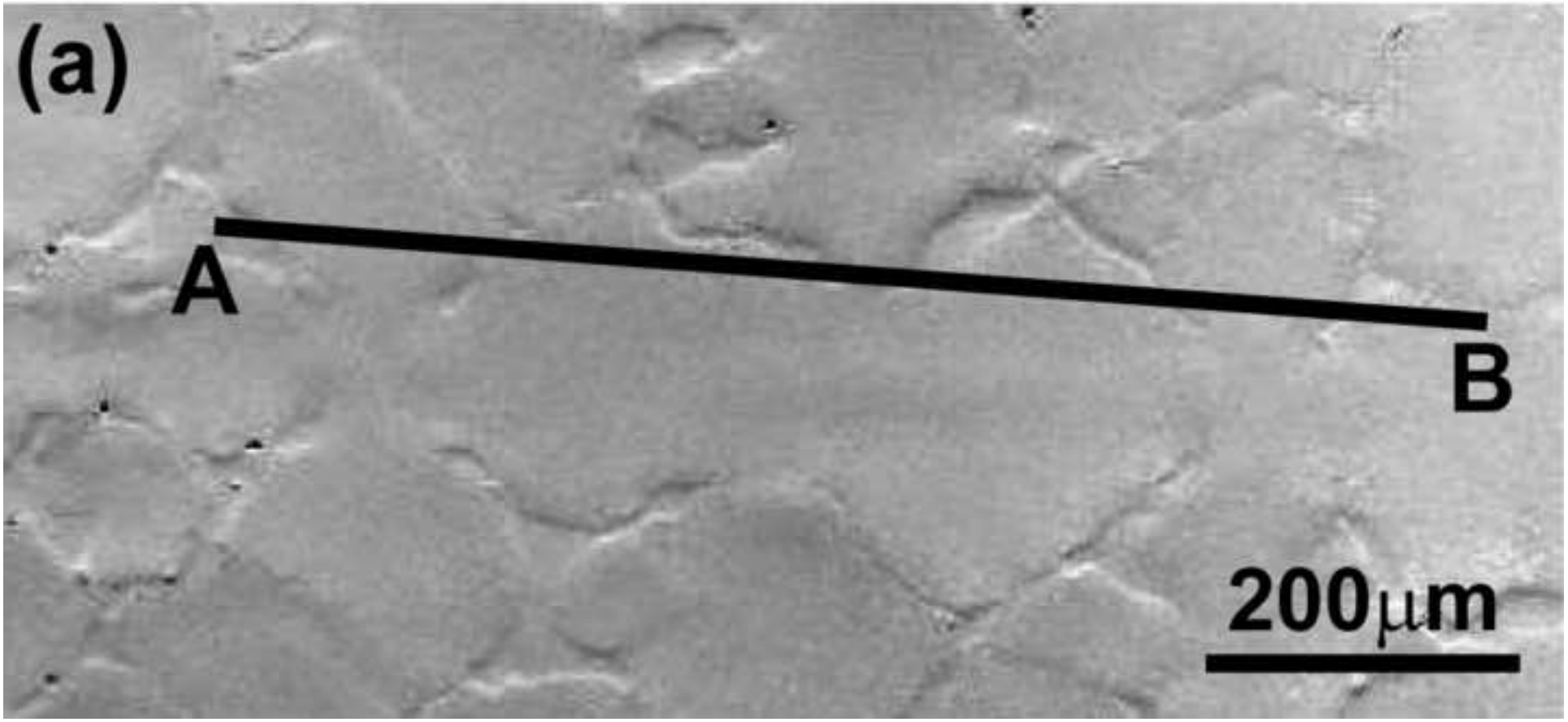

Fig.8b Local misorientation map of the same area in Fig. 8a

Click here to download high resolution image

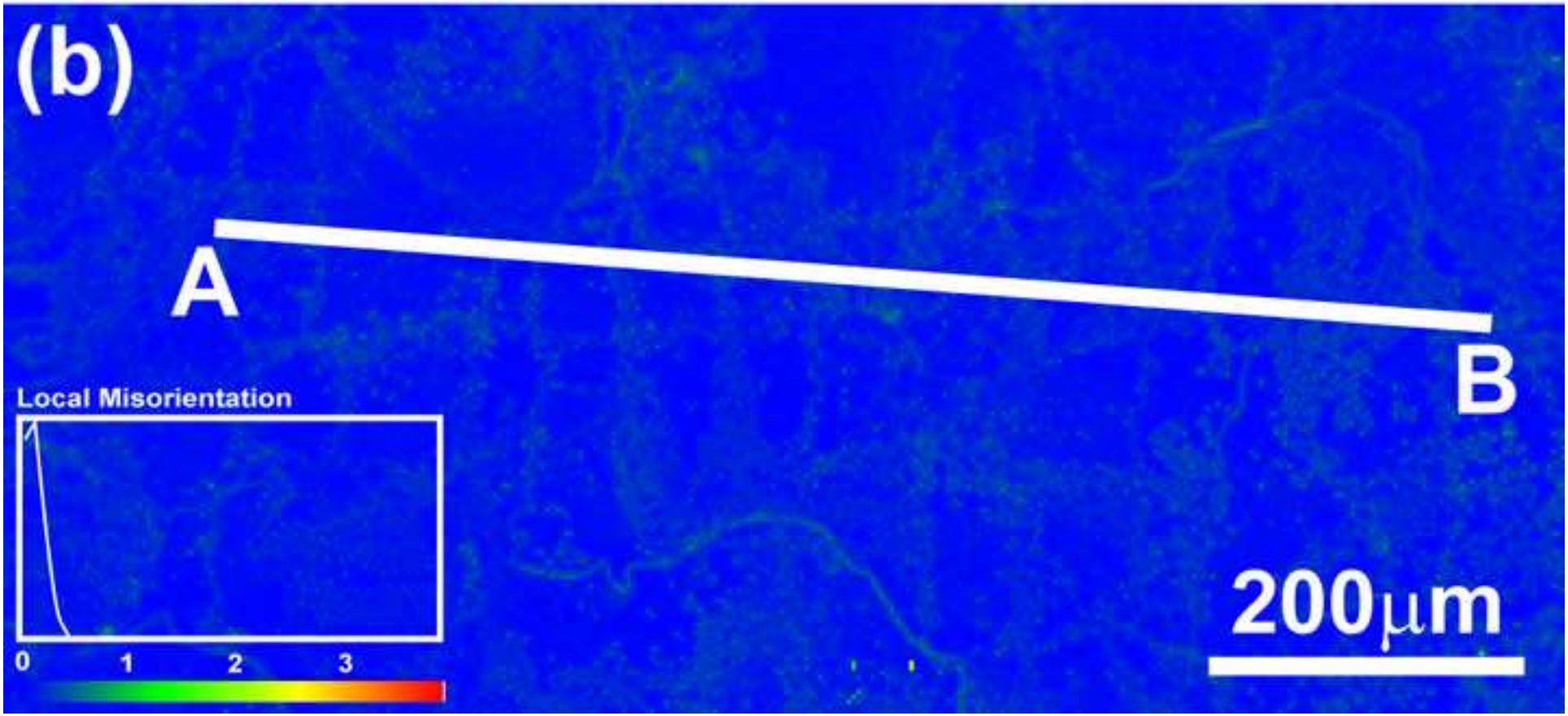

Fig.8c Accumulative misorientation profile along line AB in 8a

Click here to download high resolution image

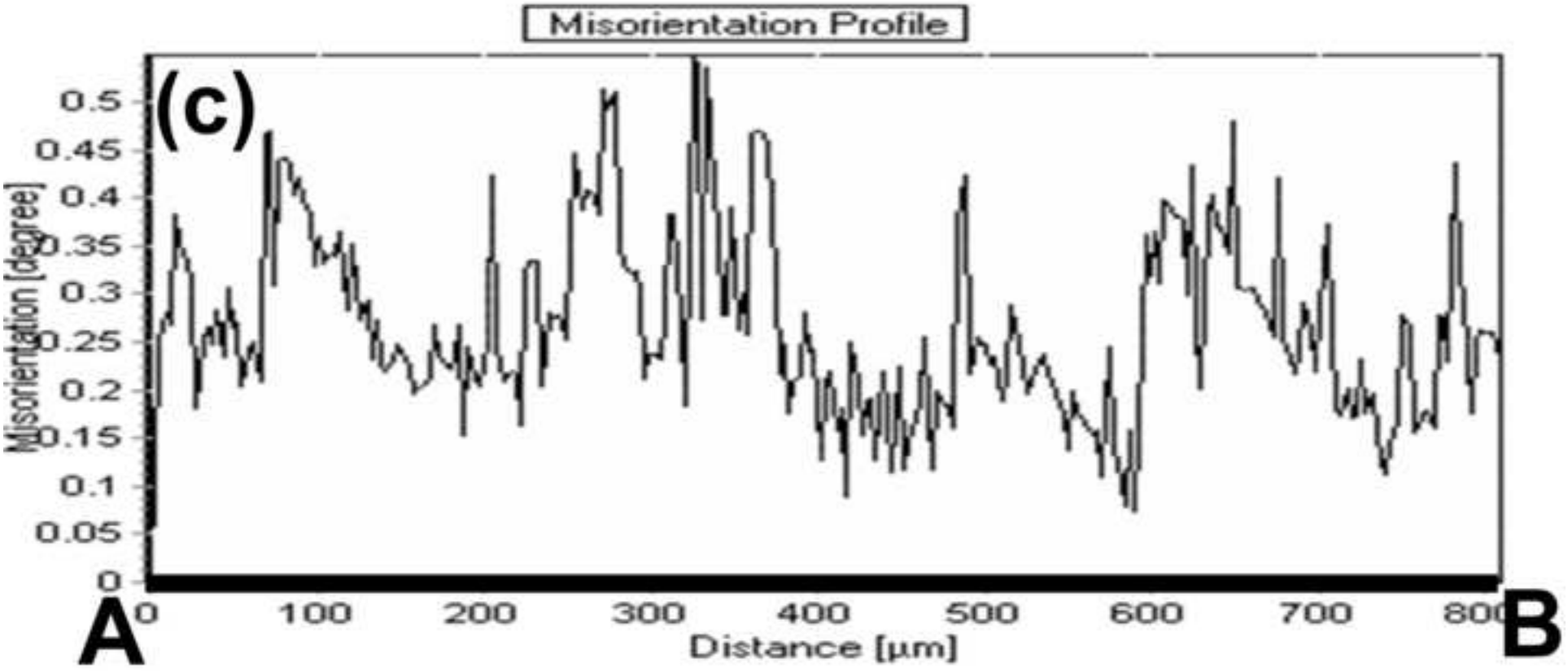

Fig.9 Dislocations in the matrix of the as-cast sample

Click here to download high resolution image